CHINESE OPTICS LETTERS

Vol. 20, No. 4 | April 2022

Spintronic terahertz emitter with integrated electromagnetic control

Yunqing Jiang (姜芸青)[1,2], Xiaoqiang Zhang (张晓强)[1,2*], Yongshan Liu (刘永山)[1,2], Pierre Vallobra[1], Sylvain Eimer[1], Fan Zhang (张 帆)[1,2], Yinchang Du (杜寅昌)[2,3], Fengguang Liu (刘风光)[1,2], Yong Xu (许 涌)[1,2**], and Weisheng Zhao (赵巍胜)[1,2***]

[1] School of Integrated Circuit Science and Engineering, Hefei Innovation Research Insititute, Beihang University, Beijing 100191, China

[2] Anhui High Reliability Chips Engineering Laboratory, Hefei 230013, China

[3] Key Laboratory of Geospace Environment, University of Science and Technology of China, Hefei 230026, China

*Corresponding author: xqzhang@buaa.edu.cn

**Corresponding author: yongxu@buaa.edu.cn

***Corresponding author: weisheng.zhao@buaa.edu.cn

Received December 10, 2021 | Accepted February 16, 2022 | Posted Online March 9, 2022

Spintronic thin films are considered as one of the promising terahertz (THz) source candidates, owing to their high performance and low cost. Much effort has been made to achieve spintronic THz sources with broadband and high conversion efficiency. However, the development of spintronic THz emitters with good compatibility, low cost, and miniaturized technology still faces many challenges. Therefore, it is urgent to extend commercial and portable spintronic THz emitters to satisfy many practical applications. Herein, we design a new generation of spintronic THz emitters composed of an alternating electromagnet and a miniaturized electronic controller. Not only can this new type of spintronic THz emitter largely simplify the ancillary equipment for spintronic sources, it also has a twice larger THz signal compared to the traditional THz time-domain spectroscopy systems with a mechanical chopper. Experimental results and theoretical calculations for electromagnetic coils show that our design can stably generate THz signals that are independent of the frequency and magnetic field of alternating signals. As the spin thin film is optimized, a magnetic field as low as 75 G satisfies the requirement for high performance THz emission. Hence, not only is the efficiency of the pump power enhanced, but also the driving current in the electromagnet is decreased. We believe that it has a wide range of applications and profound implications in THz technology based on spintronic emitters in the future.

Keywords: spintronic THz emitters; trilayer heterostructure; electromagnet; electrically driven control.
DOI: 10.3788/COL202220.043201

1. Introduction

The research of terahertz (THz) technologies provides fascinating paths for imaging[1–5], biomedicine[6–8], optical frequency combs[9,10], communication[11,12], and security diagnosis[1,13,14]. Thus, researches on strong and broadband THz emitters have earned considerable attentions[15]. Nowadays, the commercial THz source is mainly photoconductive antennas (PCAs), due to its integration and miniaturization. However, there are huge limitations on the cost, bandwidth, and conversion efficiency for commercial PCAs[16]. In the past decade, steps have been taken to ameliorate the situation. Different nano-electrode structures via plasmonic field enhancement to improve the optical-to-THz conversion efficiency[17,18], as well as various photoconductive materials for excellent carrier mobility[19] and breakdown voltage[20], have been investigated. Although these researches have made a great progress on PCA THz emitters, it is difficult for complex materials and nano-structures to be applied in extensive commerce. Another important constraint is the high optical pump power. Considering a nonlinear increase, the output THz power reaches saturation with the increase of pump power[21], and many interdigitated electrode structures on the THz emitter are studied for efficient incidence of the optical pump[22,23]. A large emitter area, however, causes a higher bias voltage and phase interference problems compared to a point source.

Based on inverse spin Hall effect (ISHE)[24,25], where an out-of-plane-directed spin current $\vec{j}_s$ is converted into an in-plane charge current $\vec{j}_c$, the spintronic THz emitters (STEs) subsequently open up new prospects owing to their energy efficiency and low cost. In the multilayer heterostructures

© 2022 Chinese Optics Letters

consisting of ferromagnetic (FM) and non-FM (NM) metal thin films, ultrafast photo-induced spin currents can be converted into ultrashort pulse charge currents, yielding the THz radiation. Works on multilayers for the generation of spintronic THz signals have been widely reported, such as Co/Pt[26], TbFe/Pt[27], W/CoFeB/Pt[28–30], and topological insulator/FM layer[31–35]. Therefore, the trilayer structure, compared with bilayer, makes full use of spin current diffusion on the double interface, which can enhance conversion efficiency of the charge current. In 2013, the exploratory research on double-layer spin thin film obtained a weak THz signal and the performance among different heavy metals[36]. Thereafter, Seifert *et al.* investigated a new generation of trilayer heterostructures as the spin thin film structure, wherein this structure not only improves the performance of THz signals, but also widens the bandwidth to 30 THz[28]. Recently, Sun *et al.*[31] reported that a novel interlayer structure between a topological insulator and ferromagnet could achieve more efficient spin-charge interconversions. However, it is costly to implement this technology on a mass basis so far. Unlike complex structures, an FM metal thin film stack structure as a THz source qualifies the demand for cost-effective and reliable technology of prominent THz signal and bandwidth. In addition, at present, the existing THz time-domain spectroscopy (TDS) systems based on spintronic THz sources are usually set up in free space[37,38]. Thus, a lot of external equipment with high cost and large size is needed, e.g., the mechanical chopper and its controller[39]. Considering the complex ancillaries for spintronic THz sources, commercially marketed as portable equipment, is a burning question, whereas studies on STEs for portability and energy efficiency are lacking in the main literature. Gueckstock *et al.*[40] combined a permanent magnet with a square wave for modulating THz polarization. However, THz polarization is a sinusoidal wave with the change of a single sinusoidal electromagnet. It is difficult to create a specific polar angle.

In this work, we design a unique structure for encapsulating STEs composed of a W/CoFeB/Pt trilayer heterostructure to enhance the pump power efficiency and downsize the external equipment. Thus, spintronic emitters can be expected to be used for PCAs to become new portable THz sources, which provide more possible optical paths for THz research, such as radar and angular deflection. In our THz-TDS system, the cumbersome mechanical chopper and its controller are replaced by an electromagnet composed of two electromagnetic coils and a function generator circuit module, which are with low cost, compact, compatible, and highly efficient. Furthermore, the generated THz signal is doubled, and the laser energy efficiency is improved simultaneously. Besides, this design can potentially serve as a more efficient THz polarization controller via integrating two orthogonal electromagnetic fields. Using the generator circuit module, not only can the sinusoidal THz polarization be created easily, but also the specific polar angle can be set by switching the alternative current to the direct current (DC). The new electrically driven module can also be expanded to other types of STEs.

2. Results and Discussion

A sketch of the device structure used for THz emission is shown in Fig. 1. In our design, the STEs fixed in an alternating electromagnetic field generate THz pulses upon the spatial photoexcitation of an 800 nm femtosecond laser. We electro-optically sample the generated THz pulses emitted by the charge current $\vec{j}_c$[36,41,42]. The details of the sample and electromagnetic coils are discussed in Supplementary Materials. A series of alternative electromagnetic fields are selected in our experiment, such as square waves with different frequencies and different amplitudes. Significantly, the necessary but cumbersome equipment in the traditional THz measurement optical system, such as the chopper that is used to modulate the pump laser and the external magnet used to magnetize the FM layer of the STEs, is successfully replaced by the alternating magnetic field induced by the two electromagnetic coils.

Figure 2(a) shows the main circuit diagram of a power supply system to generate an alternating electromagnetic field. As shown in Fig. 2(a) and Fig. S2(e) in Supplementary Materials, the power system is mainly composed of a function generator, a power amplifier, and a voltage source. In the power supply

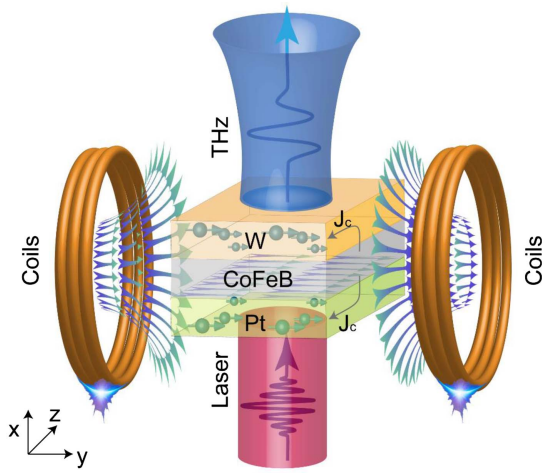

Fig. 1. Schematic of spintronic film THz emission with alternating electromagnetic coils.

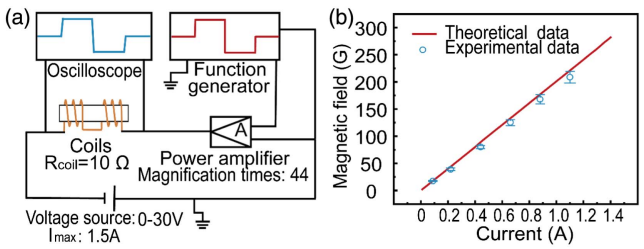

Fig. 2. (a) Power supply circuit for the electromagnetic coils to produce the alternating magnetic field. (b) Magnetic field versus current and corresponding theoretical calculation for electromagnetic coils.

system, the function generator is connected to the circuit to supply a small pulse signal with adjustable frequency and amplitude. Then, the small signal is amplified 44 times by a power amplifier, which is connected to the voltage source. As a result, an amplified pulse signal supplies the two electromagnetic coils, and an alternating magnetic field is induced. The hand-made coils are used in the system and are supervised by an oscilloscope, as shown in Fig. 2(a). The preparation and theoretical calculation of the electromagnetic coils are given in Supplementary Materials. To verify the reliability of the generated magnetic field, a comparison with the theoretical value is exhibited in Fig. 2(b), where the abscissa is current, corresponding to the amplitude from the oscilloscope. It is easy to see that the value of the generated magnetic field is comparable to the theoretical calculation, as well as increasing linearly with the current flowing in the coils.

In Fig. 3(a), with the wave signal from the function generator reversing, the signal in the coils reverses at the same time when supervised by the oscilloscope. In fact, a small delay ($< 4\,\mu s$) of the voltage signal occurs between the command from the function generator and the generated alternating magnetic field, and it could be ignored. From the oscilloscope, we can find that the waveform in the circuit almost stays consistent with the function generator. Then, the periodic signal can be used for equivalent-time sampling. Based on the equivalent-time sampling technique, a periodic signal is required for implementing THz time-domain waveform measurements[43–45], and, in general, a chopper is selected to provide the periodic signals. For better understanding, a sketch of the chopper with a duty cycle of 50% used for pump laser modulation is shown in Fig. 3(b) (the detailed procedure is shown in Supplementary Materials), and its frequency is 184 Hz. Generally speaking, the chopper can only provide a square pulse, and then the low level output is zero [see blue line in Fig. 3(b)]. The pump laser is underutilized in the THz signal test system during the period of low level (0). For the sake of more sufficient energy utilization, the chopper is replaced by applying an alternating square wave signal with a frequency of 184 Hz [see orange dash line in Fig. 3(b)]. In this case, an alternating current with square wave flows through the electromagnetic coils, meaning that there are two opposite directions magnetized in the FM layer in one period. Therefore, the connection between THz emission and magnetization is shown as follows[36,40,46]:

$$E_{\mathrm{THz}} \propto M \times u_x, \tag{1}$$

where E_{THz} is the electric field intensity of the THz signal, M is the FM magnetization, and u_x is the unit vector along the x axis in Fig. 1. Thus, the measured value of the THz signal is equal to $E_{\mathrm{THz}} - (-E_{\mathrm{THz}})$ based on the equivalent-time sampling. This results in a generated THz signal that can be detected, as shown in Fig. 3(c) (orange line). It is interesting that the generated THz signal via electromagnetic modulation is 2 times larger than the chopper-modulated one under the same pump laser. This mechanism can be applied to other fields like photoconductive switches. We also find that the electromagnetic coils are compatible with the traditional chopper. As shown in Fig. 3(c), two THz signal waveforms (blue line and gray dash line) are measured by a THz emission system with a chopper, where two reversed directions of DC flow in the coils, respectively. We conclude that the STEs integrated with two electromagnetic coils are compatible with the common chopper. The details of the experiment can be seen in Supplementary Materials. In a comparison of the traditional chopper and its controller in Supplementary Materials Fig. S2(a)–S2(c), the miniaturized circuit module [in Supplementary Materials Fig. S2(e)] is 5 times smaller. Besides, the STEs with electromagnetic coils [in Supplementary Materials Fig. S2(d)] can save more space than permanent magnets.

Moreover, the STEs integrated with two electromagnetic coils are flexible for adjusting the phase of the generated THz signal. As shown in Fig. 3(c), the THz signal (the gray dash line) phase becomes opposite when an opposite DC is applied on the electromagnet. It meets the expectation that upon reversing the direction of the magnetic field, the generated THz signal experiences a sign reversal. Figure 3(d) shows the generated THz signal when the alternating voltage starts at a different level (1 or −1). In Fig. 3(d), the orange line represents the THz signal when the alternating voltage starts at the high level (1). Conversely, the gray line represents the THz signal when the alternating voltage starts at the low level (−1). We can find that the generated THz signal experiences a sign reversal because of the sign reversal of the generated magnetic field. Therefore, in our system, we can easily switch the starting level by programming the function generator to yield two opposite signs of THz

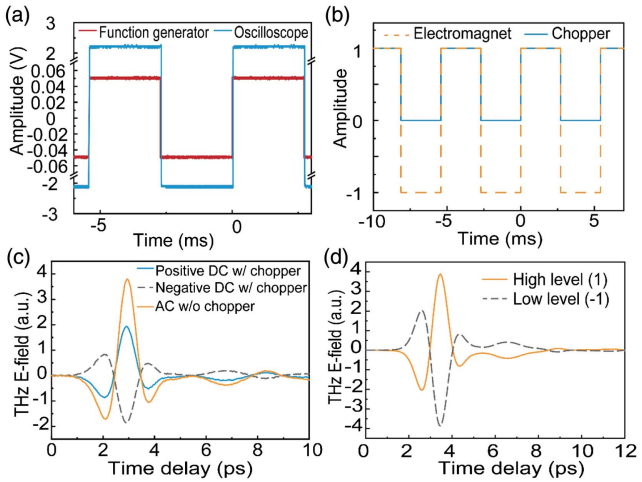

Fig. 3. (a) Square waveforms detected from the function generator and the oscilloscope. (b) Simplified waveforms for laser modulation by a chopper and electromagnetic field modulation by a function generator. (c) THz signal waveforms from the W/CoFeB/Pt spintronic film measured by a THz emission system, where two reverse directions of the direct current (DC) and alternating current (AC) flow in coils with chopper (w/ chopper) and without chopper (w/o chopper), respectively. (d) THz signal waveforms from the W/CoFeB/Pt spintronic emitter with the original start level (orange line) and a π phase difference start level (gray dash line).

signals. In other words, we can say that the π phase difference of the generated THz signals via electric control can be achieved easily and efficiently in this system, which is promising in THz communication.

Lastly, THz signals are surveyed in the W/CoFeB/Pt sample with different frequencies of alternating voltage applied on the electromagnet [Fig. 4(a)]. It is worth mentioning that the peak value of the THz wave is relatively stable below 1 kHz. In addition, we measured the THz field with a 2 mm thick ZnTe crystal in a N_2 atmosphere, whose bandwidth extends from 1 to 2.5 THz. Figure S3 of Supplementary Materials shows the corresponding amplitude spectra of THz signals from the STE via the fast Fourier transform at the frequency. Above 1 kHz, the peak value of the THz wave decreases with the increase of the frequency, but the shape of the THz waveform remains unchanged. The peak values of the THz signal extracted from Fig. 4(a) are plotted in Fig. 4(b).

There is an obvious inflection point around 1884 Hz and a sharp fall after it [see fitting curve in Fig. 4(b)]. Besides, a 67% drop from 984 Hz to 6884 Hz is observed in Fig. 4(b). This illustrates the negative effects of the electromagnet on the THz signal when the frequency applied on the electromagnet exceeds the repetition rate of the laser pulses. The alternating magnetic fields with different intensities are further investigated via changing the amplitude of the square voltage on the electromagnet from 2 mV to 300 mV, which is the voltage on the coils before amplification. It can convert into the current and magnetic field by the Biot–Savart law in Supplementary Materials. As shown in Fig. 4(c), the THz waveforms under different voltages remain their shapes. Although the peak value of the THz signal, shown in Fig. 4(d), increases sharply with the increase of the magnetic field, it is relatively stable above the saturation field (100 mV). Because the magnetic field cannot fully magnetize the FM layer when below the saturation magnetic field, the weaker magnetic field is used, and the current creates less charge[36]. Note that the peak value of the THz signal is independent of the electromagnet voltage after reaching the saturation field. According to the experiment data in Fig. 2(b), the saturation field value is exceedingly low (75 G), indicating the STEs work even with a low magnetic field. In terms of electromagnetic coils, a smaller current flowing in them avoids more serious heat. Avoiding unwanted heating for the instruments in practical application not only extends the service life but saves energy.

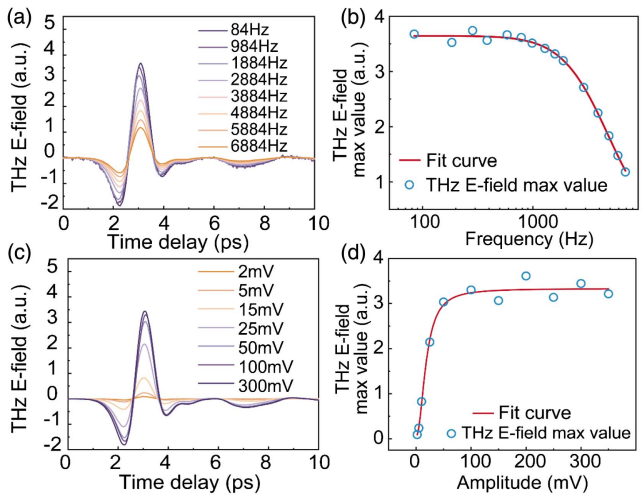

Fig. 4. (a) THz signal waveforms and (b) the peak value of the THz signal under different frequencies from 84 Hz to 6884 Hz. (c) THz signal waveforms and (d) the peak value of the THz signal under different square wave amplitudes from 2 mV to 300 mV.

3. Conclusions

In conclusion, we have exhibited a novel miniaturization circuit design for a W/CoFeB/Pt sandwich heterostructure as a potential commercial THz emitter. The superiority of an alternating electromagnet with a miniaturized control circuit has been studied by comparing it with the cumbersome chopper in the THz-TDS system. Through the special design, a 2 times larger THz time-domain signal is obtained on a spin thin film, indicating full utilization of the pump power in comparison to a traditional THz-TDS system. Note that a small magnetic field, 40 G, can allow the spin thin film to generate a THz signal, meaning that a small space and current can meet the requirements for a drive circuit. Simultaneously, we have demonstrated the stability of our STE below 1 kHz square wave signal modulation, while a modulation frequency higher than the repetition rate of the laser has a negative effect on the performance of the emitter. The demonstration is based on the common spin thin film, but the approach of curtailing the STE space can be efficiently applied in both free space and optical-fiber systems. Therefore, our design is a promising route for further development of THz applications.

Acknowledgement

This work was supported by the National Natural Science Foundation of China (Nos. 12004025 and 11904016) and Beihang Hefei Innovation Research Institute Project (No. BHKX-19-01). We acknowledge support from Key Laboratory of Geospace Environment, University of Science and Technology of China, Chinese Academy of Sciences.

References

1. C. M. Watts, D. Shrekenhamer, J. Montoya, G. Lipworth, J. Hunt, T. Sleasman, S. Krishna, D. R. Smith, and W. J. Padilla, "Terahertz compressive imaging with metamaterial spatial light modulators," Nat. Photonics **8**, 605 (2014).
2. S.-C. Chen, Z. Feng, J. Li, W. Tan, L.-H. Du, J. Cai, Y. Ma, K. He, H. Ding, Z.-H. Zhai, Z.-R. Li, C.-W. Qiu, X.-C. Zhang, and L.-G. Zhu, "Ghost spintronic THz-emitter-array microscope," Light Sci. Appl. **9**, 99 (2020).
3. H. Guerboukha, Y. Amarasinghe, R. Shrestha, A. Pizzuto, and D. M. Mittleman, "High-volume rapid prototyping technique for terahertz metallic metasurfaces," Opt. Express **29**, 13806 (2021).
4. D. M. Mittleman, "Twenty years of terahertz imaging [Invited]," Opt. Express **26**, 9417 (2018).

5. W. L. Chan, J. Deibel, and D. M. Mittleman, "Imaging with terahertz radiation," Rep. Prog. Phys. **70**, 1325 (2007).
6. A. P. Gong, Y. T. Qiu, X. W. Chen, Z. Y. Zhao, L. Z. Xia, and Y. N. Shao, "Biomedical applications of terahertz technology," Appl. Spectrosc. Rev. **55**, 418 (2020).
7. M. Wan, J. J. Healy, and J. T. Sheridan, "Terahertz phase imaging and biomedical applications," Opt. Laser Technol. **122**, 105859 (2020).
8. L. Sun, Z. Zhou, J. Zhong, Z. Shi, Y. Mao, H. Li, J. Cao, and T. H. Tao, "Implantable, degradable, therapeutic terahertz metamaterial devices," Small **16**, 2000294 (2020).
9. H. Li, M. Yan, W. Wan, T. Zhou, K. Zhou, Z. Li, J. Cao, Q. Yu, K. Zhang, M. Li, J. Nan, B. He, and H. Zeng, "Graphene-coupled terahertz semiconductor lasers for enhanced passive frequency comb operation," Adv. Sci. **6**, 1900460 (2019).
10. H. Li, Z. Li, W. Wan, K. Zhou, X. Liao, S. Yang, C. Wang, J. C. Cao, and H. Zeng, "Toward compact and real-time terahertz dual-comb spectroscopy employing a self-detection scheme," ACS Photonics **7**, 49 (2020).
11. T. Nagatsuma, S. Horiguchi, Y. Minamikata, Y. Yoshimizu, S. Hisatake, S. Kuwano, N. Yoshimoto, J. Terada, and H. Takahashi, "Terahertz wireless communications based on photonics technologies," Opt. Express **21**, 23736 (2013).
12. J. Ma, R. Shrestha, J. Adelberg, C.-Y. Yeh, Z. Hossain, E. Knightly, J. M. Jornet, and D. M. Mittleman, "Security and eavesdropping in terahertz wireless links," Nature **563**, 89 (2018).
13. D. Molter, D. Huebsch, T. Sprenger, K. Hens, K. Nalpantidis, F. Platte, G. Torosyan, R. Beigang, J. Jonuscheit, G. von Freymann, and F. Ellrich, "Mail inspection based on terahertz time-domain spectroscopy," Appl. Sci. **11**, 950 (2021).
14. Y. Takida, K. Nawata, and H. Minamide, "Security screening system based on terahertz-wave spectroscopic gas detection," Opt. Express **29**, 2529 (2021).
15. M. Tal, S. Keren-Zur, and T. Ellenbogen, "Nonlinear plasmonic metasurface terahertz emitters for compact terahertz spectroscopy systems," ACS Photonics **7**, 3286 (2020).
16. N. M. Burford and M. O. El-Shenawee, "Review of terahertz photoconductive antenna technology," Opt. Eng. **56**, 010901 (2017).
17. B. Heshmat, H. Pahlevaninezhad, Y. Pang, M. Masnadi-Shirazi, R. B. Lewis, T. Tiedje, R. Gordon, and T. E. Darcie, "Nanoplasmonic terahertz photoconductive switch on GaAs," Nano Lett. **12**, 6255 (2012).
18. K. Moon, I.-M. Lee, J.-H. Shin, E. S. Lee, N. Kim, W.-H. Lee, H. Ko, S.-P. Han, and K. H. Park, "Bias field tailored plasmonic nano-electrode for high-power terahertz photonic devices," Sci. Rep. **5**, 13817 (2015).
19. A. Jooshesh, V. Bahrami-Yekta, J. Zhang, T. Tiedje, T. E. Darcie, and R. Gordon, "Plasmon-enhanced below bandgap photoconductive terahertz generation and detection," Nano Lett. **15**, 8306 (2015).
20. K. Moon, J. Choi, J.-H. Shin, S.-P. Han, H. Ko, N. Kim, J.-W. Park, Y.-J. Yoon, K.-Y. Kang, H.-C. Ryu, and K. H. Park, "Generation and detection of terahertz waves using low-temperature-grown GaAs with an annealing process," ETRI J. **36**, 159 (2014).
21. D. S. Kim and D. S. Citrin, "Coulomb and radiation screening in photoconductive terahertz sources," Appl. Phys. Lett. **88**, 161117 (2006).
22. A. Singh and S. S. Prabhu, "Microlensless interdigitated photoconductive terahertz emitters," Opt. Express **23**, 1529 (2015).
23. N. T. Yardimci, S.-H. Yang, C. W. Berry, and M. Jarrahi, "High-power terahertz generation using large-area plasmonic photoconductive emitters," IEEE Trans. Terahertz Sci. Technol. **5**, 223 (2015).
24. S. O. Valenzuela and M. Tinkham, "Direct electronic measurement of the spin Hall effect," Nature **442**, 176 (2006).
25. Y. Xu, F. Zhang, X.-Q. Zhang, Y.-C. Du, H.-H. Zhao, T.-X. Nie, X.-J. Wu, and W.-S. Zhao, "Research advances in spintronic terahertz sources," Acta Phys. Sin. **69**, 200703 (2020).
26. T. J. Huisman, R. V. Mikhaylovskiy, J. D. Costa, F. Freimuth, E. Paz, J. Ventura, P. P. Freitas, S. Blugel, Y. Mokrousov, T. Rasing, and A. V. Kimel, "Femtosecond control of electric currents in metallic ferromagnetic heterostructures," Nat. Nanotechnol. **11**, 455 (2016).
27. R. Schneider, M. Fix, R. Heming, S. Michaelis de Vasconcellos, M. Albrecht, and R. Bratschitsch, "Magnetic-field-dependent THz emission of spintronic TbFe/Pt layers," ACS Photonics **5**, 3936 (2018).
28. T. Seifert, S. Jaiswal, U. Martens, J. Hannegan, L. Braun, P. Maldonado, F. Freimuth, A. Kronenberg, J. Henrizi, I. Radu, E. Beaurepaire, Y. Mokrousov, P. M. Oppeneer, M. Jourdan, G. Jakob, D. Turchinovich, L. M. Hayden, M. Wolf, M. Munzenberg, M. Klaui, and T. Kampfrath, "Efficient metallic spintronic emitters of ultrabroadband terahertz radiation," Nat. Photonics **10**, 483 (2016).
29. U. Nandi, M. S. Abdelaziz, S. Jaiswal, G. Jakob, O. Gueckstock, S. M. Rouzegar, T. S. Seifert, M. Klaeui, T. Kampfrath, and S. Preu, "Antenna-coupled spintronic terahertz emitters driven by a 1550 nm femtosecond laser oscillator," Appl. Phys. Lett. **115**, 022405 (2019).
30. D. Kong, X. Wu, B. Wang, T. Nie, M. Xiao, C. Pandey, Y. Gao, L. Wen, W. Zhao, C. Ruan, J. Miao, Y. Li, and L. Wang, "Broadband spintronic terahertz emitter with magnetic-field manipulated polarizations," Adv. Opt. Mater. **7**, 1900487 (2019).
31. R. Sun, S. Yang, X. Yang, E. Vetter, D. Sun, N. Li, L. Su, Y. Li, Y. Li, Z.-Z. Gong, Z.-K. Xie, K.-Y. Hou, Q. Gul, W. He, X.-Q. Zhang, and Z.-H. Cheng, "Large tunable spin-to-charge conversion induced by hybrid Rashba and Dirac surface states in topological insulator heterostructures," Nano Lett. **19**, 4420 (2019).
32. Y. Zeng, U. Chattopadhyay, B. Zhu, B. Qiang, J. Li, Y. Jin, L. Li, A. G. Davies, E. H. Linfield, B. Zhang, Y. Chong, and Q. J. Wang, "Electrically pumped topological laser with valley edge modes," Nature **578**, 246 (2020).
33. X. Wang, L. Cheng, D. Zhu, Y. Wu, M. Chen, Y. Wang, D. Zhao, C. B. Boothroyd, Y. M. Lam, J.-X. Zhu, M. Battiato, J. C. W. Song, H. Yang, and E. E. M. Chia, "Ultrafast spin-to-charge conversion at the surface of topological insulator thin films," Adv. Mater. **30**, 1802356 (2018).
34. P. Seifert, K. Vaklinova, S. Ganichev, K. Kern, M. Burghard, and A. W. Holleitner, "Spin Hall photoconductance in a three-dimensional topological insulator at room temperature," Nat. Commun. **9**, 331 (2018).
35. H. Zhao, X. Chen, C. Ouyang, H. Wang, D. Kong, P. Yang, B. Zhang, C. Wang, G. Wei, T. Nie, W. Zhao, J. Miao, Y. Li, L. Wang, and X. Wu, "Generation and manipulation of chiral terahertz waves in the three-dimensional topological insulator Bi_2Te_3," Adv. Photonics **2**, 066003 (2020).
36. T. Kampfrath, M. Battiato, P. Maldonado, G. Eilers, J. Noetzold, S. Maehrlein, V. Zbarsky, F. Freimuth, Y. Mokrousov, S. Bluegel, M. Wolf, I. Radu, P. M. Oppeneer, and M. Muenzenberg, "Terahertz spin current pulses controlled by magnetic heterostructures," Nat. Nanotechnol. **8**, 256 (2013).
37. W. Jia, M. Liu, Y. Lu, X. Feng, Q. Wang, X. Zhang, Y. Ni, F. Hu, M. Gong, X. Xu, Y. Huang, W. Zhang, Y. Yang, and J. Han, "Broadband terahertz wave generation from an epsilon-near-zero material," Light Sci. Appl. **10**, 11 (2021).
38. M. Chen, K. Lee, J. Li, L. Cheng, Q. Wang, K. Cai, E. E. M. Chia, H. Chang, and H. Yang, "Anisotropic picosecond spin-photocurrent from Weyl semimetal WTe_2," ACS Nano **14**, 3539 (2020).
39. X. Chen, X. Wu, S. Shan, F. Guo, D. Kong, C. Wang, T. Nie, C. Pandey, L. Wen, W. Zhao, C. Ruan, J. Miao, Y. Li, and L. Wang, "Generation and manipulation of chiral broadband terahertz waves from cascade spintronic terahertz emitters," Appl. Phys. Lett. **115**, 221104 (2019).
40. O. Gueckstock, L. Nádvorník, T. S. Seifert, M. Borchert, G. Jakob, G. Schmidt, G. Woltersdorf, M. Kläui, M. Wolf, and T. Kampfrath, "Modulating the polarization of broadband terahertz pulses from a spintronic emitter at rates up to 10 kHz," Optica **8**, 1013 (2021).
41. S. O. Valenzuela and M. Tinkham, "Direct electronic measurement of the spin Hall effect," Nature **442**, 176 (2006).
42. O. Mosendz, J. E. Pearson, F. Y. Fradin, G. E. W. Bauer, S. D. Bader, and A. Hoffmann, "Quantifying spin Hall angles from spin pumping: experiments and theory," Phys. Rev. Lett. **104**, 046601 (2010).
43. P. U. Jepsen, D. G. Cooke, and M. Koch, "Terahertz spectroscopy and imaging-modern techniques and applications," Laser Photonics Rev. **5**, 124 (2011).
44. K. Ahi, S. Shahbazmohamadi, and N. Asadizanjani, "Quality control and authentication of packaged integrated circuits using enhanced-spatial-resolution terahertz time-domain spectroscopy and imaging," Opt. Lasers Eng. **104**, 274 (2018).
45. H. Guerboukha, K. Nallappan, and M. Skorobogatiy, "Toward real-time terahertz imaging," Adv. Opt. Photonics **10**, 843 (2018).
46. Q. Zhang, Z. Luo, H. Li, Y. Yang, X. Zhang, and Y. Wu, "Terahertz emission from anomalous Hall effect in a single-layer ferromagnet," Phys. Rev. Appl. **12**, 054027 (2019).